COMMUNICATION

CLINICAL ANATOMY **WILEY**

Blood supply to the superficial fascia of the abdomen: An anatomical study

Carmelo Pirri[1] | **Lucia Petrelli**[1] | **Caterina Fede**[1] | **Diego Guidolin**[1] | **Cesare Tiengo**[2] | **Raffaele De Caro**[1] | **Carla Stecco**[1]

[1]Department of Neurosciences, Institute of Human Anatomy, University of Padova, Padova, Italy

[2]Department of Neurosciences, The Plastic Surgery Unit of the University of Padova Medical Center, Padova, Italy

Correspondence
Carmelo Pirri, Department of Neurosciences, Institute of Human Anatomy, University of Padova, Via Gabelli 67, 35121, Padova, Italy.
Email: carmelop87@hotmail.it

Abstract

The aim of this study was to examine data demonstrating that Scarpa's fascia, a superficial fascia of the anterior abdominal wall, is a vascularized tissue. Specimens of the fascia of seven volunteers undergoing abdominoplasty surgical procedures at the Plastic Surgery Unit of the University of Padova Medical Center were collected. Fractal analysis and quantitative assessment of the vascular network of the fascia was carried out, exploiting the presence of blood in the vessels. Each sample was divided and processed for histological/immunohistochemical analysis (into 5 micron-paraffin embedded sections and cryo-sectioned free-floating samples) as well as for electron microscopy study. A rich vascular pattern forming a fine, dense meshwork with an area percentage of 6.20% ± 2.10% von Willebrand factor stained vessels was noted in all the specimens of the fascia examined; the area percentage of the αSMA-stained vessels was 2.93% ± 1.80%. The diameters of the vessels fell between the 13 and 65 μm range; the network was composed of arteries, veins, capillaries and lymphatic segments. Topological results showed that the vascular network within Scarpa's fascia is well branched (segments: 6615 ± 3070 and 8.40 ± 3.40 per mm^2; crossing points: 3092 ± 1490 and 3.40 ± 1.90 per mm^2). Fractal analysis (fractal dimension = 1.063 ± 0.10; lacunarity = 0.60 ± 0.10) revealed that this particular vascular network has an optimal spatial distribution and homogeneity occupying the entire space of the superficial fascia. These findings could undoubtedly be useful to plastic surgeons as well as to pain management specialists.

KEYWORDS
anterior abdominal wall, arteries, arterio-venous anastomoses, capillaries, flaps, hypodermis, lymphatics, plastic surgery, reconstructive surgery, subcutaneous tissue, superficial fascia, vascularization, veins

1 | INTRODUCTION

The superficial fascia of the anterior abdominal wall was the first superficial fascia to be studied. Antonio Scarpa (1752–1832) described it as a membrous layer that extends into the subcutaneous fat tissue in the first and second editions (1809, 1823) of his famous texts regarding the inguinal hernia. Superficial fascia has recently been demonstrated in many other areas of the body (Fede et al., 2020; Macchi et al., 2007; Pirri, Fede, Petrelli, et al., 2021; Stecco, 2015; Stecco & Duparc, 2011); it has been described as a dense collagenous

connective tissue layer of the anterior abdominal wall that divides the hypodermis into two distinct layers: the superficial adipose tissue (SAT) and the deep adipose tissue (DAT). Numerous surgical approaches have been developed using superficial fascia as flaps during plastic reconstructive surgery (Koshima et al., 1996); it has also been used as a dissection guide during superficial lymphadenectomy (Das et al., 2022) and abdominoplasty/ liposuction procedures (Novais et al., 2020).

Novais et al. (2020) recently reported that those abdominoplasty procedures during which Scarpa's fascia is preserved are characterized by beneficial effects in terms of scar quality and cutaneous sensibility with respect to other techniques. Several studies have demonstrated that Scarpa's fascia flaps can be used during deep inferior epigastric artery (DIEA) reconstruction (Koshima et al., 1989 and 1996; Southern & Ramakrishnan, 1996; Moon & Taylor, 1988; Mori, Akita & Hata, 2007). Deep inferior epigastric artery perforator (DIEP) flaps have also been used for breast reconstruction. Odobescu and Keith (2021) described a novel method of pre-shaping DIEP hemi-abdominal flaps using a one-step purse-string suture at the level of the Scarpa fascia; that method seems to improve the projection of the flap without putting any direct tension on its underside. De la Parra-Marquez et al. (2021) focused on superficial thinning of the DIEP flap to achieve an aesthetic flap-based reconstructed breast in obese patients that preserved Scarpa's fascia and deep fat. However, despite increasing interest in the superficial fascia and clear clinical evidence that the preservation of Scarpa's fascia reduces some vascular and lymphatic problems, little or no research has focused on the vascularization of this fibrous tissue, and most studies have continued to concentrate almost exclusively on the skin and the hypodermis in general (Standring, 2016). In the light of these considerations, the current study set out to assess data demonstrating that Scarpa's fascia is indeed vascularized and to describe its characteristics and organization.

2 | MATERIALS AND METHODS

2.1 | Sample collection

Samples (approximately 2×2 cm) of the superficial fascia of the abdominal wall of seven volunteer patients who were recruited at the Plastic Surgery Unit of the University of Padova Medical Center were collected (Figure 1). The samples were collected from the subumbilical region of those patients between January and April 2022 during abdominoplasty surgical procedures. Full-thickness specimens (from the skin to the deep fascia) were taken from an area approximately 3 cm below the umbilicus and 3 cm lateral to the midline. All the subjects had a BMI of 40–49.9 kg/m², which is compatible with severe obesity. All of the ethical regulations regarding research on human tissues described by Macchi et al. (2011) were carefully followed, and written informed consent was obtained from all of the patients.

The specimens were isolated and fixed in 10% formalin, dehydrated in graded ethanol and in xylene reagent to increase the vessels' visibility. They were then used to obtain images of the vascular network, exploiting the presence of blood in the vessels (Figure 2). Each sample was divided into three parts: 2×1 cm samples were used for the floating sections, 1×0.7 cm samples were used for histological and immunohistochemical analysis, and the last, small sample was utilized for transmission electron microscopy (TEM) study.

2.2 | Immunohistochemistry analysis

the specimens were embedded in paraffin and 5 μm sections were cut, dewaxed, endogenous peroxidases (H_2O_2 1% in phosphate buffered saline = PBS) blocked, incubated in blocking solution (PBS + 0.2% bovine serum albumin [BSA]) for 1 h and then incubated overnight at 4°C with primary antibodies. Vascularization detection: Rabbit anti
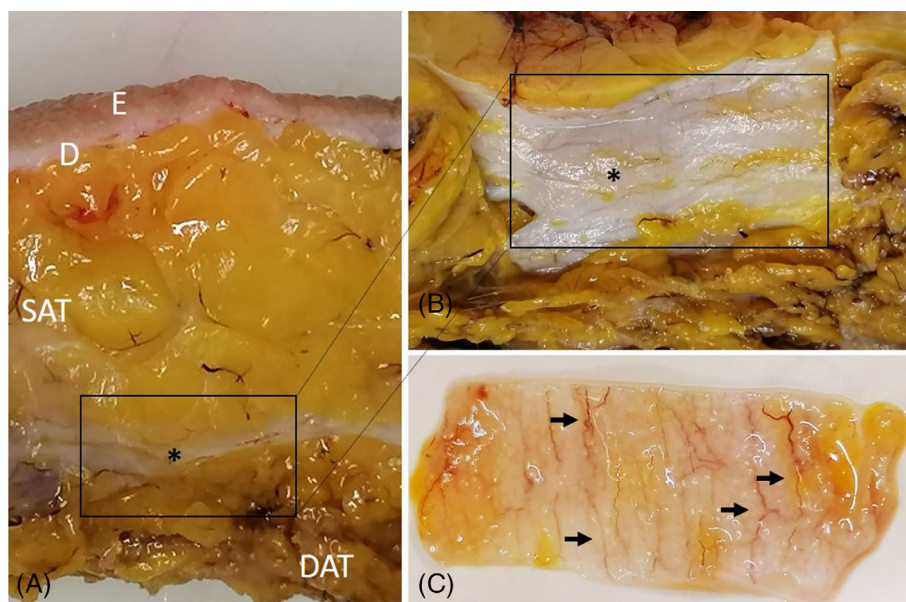

FIGURE 1 Sample collection. (A) macroscopic view of entire collected sample; (B) superficial fascia; (C) isolated sample of superficial fascia with vascular network. D, dermis; DAT, deep adipose tissue; E, epidermis; SAT, superficial adipose tissue; *, superficial fascia; arrows, examples of blood vessels (red lines)

FIGURE 2 Isolated superficial fascia with the vascular network. (A) Pre-clearing; (B) after-clearing. Arrows: examples of blood vessels
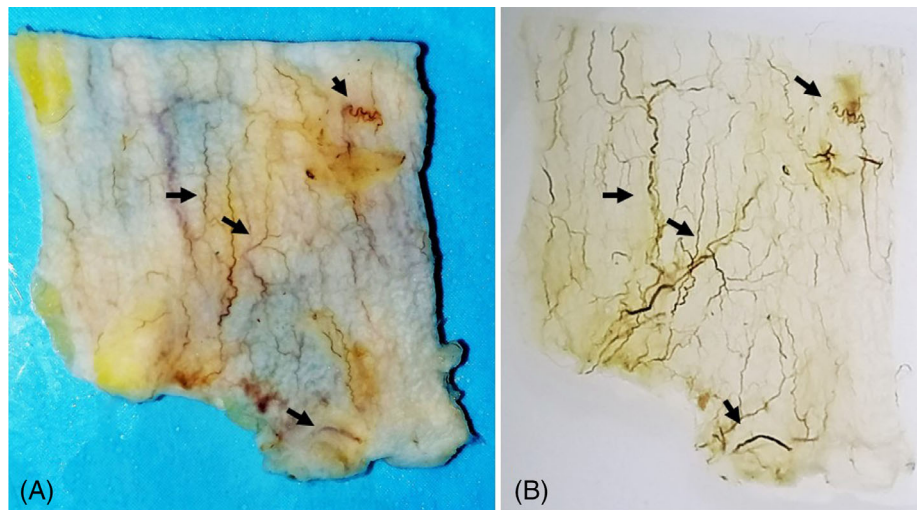
Human Von Willebrand Factor, diluted 1:600 (vWF—Agilent Dako) and mouse Anti human Smooth Muscle Actine diluted 1:200 (Clone 1A4—Agilent Dako). The free-floating sections were incubated for innervation in Rabbit Polyclonal Anti S100 diluted 1:4000 (Agilent-Dako), Rabbit Anti Tyrosine Hydroxylase dilution 1:500 (GeneTex). After repeated washings in PBS, the samples were incubated using the HRP Rabbit/Mouse secondary antibody kit Advance (Agilent Dako). Negative controls were processed using the same protocol but without the primary antibodies. The reaction was then developed with 3,3′-diaminobenzidine (Liquid DAB + substrate Chromogen System kit Dako) and stopped with distilled water; the slides were counterstained with hematoxylin.

2.3 | The free-floating sections

the samples of superficial fascia were isolated and fixed in 10% formalin overnight, washed in PBS and transferred immediately to PBS containing increasing amounts of sucrose (10%–20%–30%) for 4 days and then frozen in isopentane at −80°C in ice dry. Sections of 60 μm were cut at −20°C in a Cryostat, washed in water, and stained with hematoxylin. Some sections were stained for 20 with DAB (with 3,3′-diaminobenzidine) without the first antibody, the low background stained the vessels yellow.

2.4 | Semithin sections and TEM analysis

Small specimens were fixed in 2.5% glutaraldehyde (Agar Scientific Elektron Technology, UK) in 0.1 M phosphate buffer, post-fixed in osmium tetroxide (Agar Scientific Elektron Technology, UK), dehydrated in a graded alcohol series and then embedded in Epoxy Embedding Medium Kit (Sigma-Aldrich). Semithin and ultrathin sections were cut with an ultramicrotome RMC-PTX PowerTome (Boeckeler Instruments, Arizona –USA). The semithin sections (0.5 micron) were stained with 1% Toluidine blue on a hot plate (+80°C). The ultrathin

sections (60 nm) collected on 300-mesh copper grids were counterstained with 1% uranyl acetate and then with Sato's lead. The specimens were examined using a Hitachi H-300 TEM (Japan). The images were acquired using a Leica DMR microscope (Leica Microsystems, Wetzlar, Germany).

2.5 | Image acquisition

The images of cleared tissue samples were acquired with a stereo microscope (SZNT-T, OPTIKA, Italy) operating at a magnification of 1× and stored as digital high-resolution images (TIFF file, 3000 × 4000 pixels). Immunohistochemical sections were examined using a Leica bright-field DMR microscope (Leica Microsystems, Wetzlar, Germany) with 40× magnification; a minimum of at least 10 images per section were acquired and stored as digital high-resolution images (TIFF files, 1780 × 1220 pixels).

2.6 | Image processing and analysis

To morphometrically characterize the pattern of the vascular system of the superficial fascia, the images of the free-floating sections of the specimens underwent image processing and analysis using ImageJ software (freely available at http://rsb.info.nih.gov/ij/, (Schneider et al., 2012)). Briefly, after the shading effect was corrected, the background signals were removed, and each image was manually adjusted to eliminate non-vascular structures, a top-hat filter was applied to enhance the contrast between the pattern of the vascular vessels and the background. An adaptive discrimination procedure was then applied to select the vessel profiles. The method operates with a local threshold: the mean gray value of neighboring regions was calculated for every pixel (by a 15-pixel low-pass filter); this value plus an offset threshold constant defined the local threshold for that pixel. After the remaining artifacts were edited interactively, a binary image of the vascular network was obtained. A binary skeleton of the image was

FIGURE 3 Transformation from digital to binary and skeletonized images of vascularization within superficial fascia. (A) Full color digital image of stereo microscope field of superficial fascia vascularization after clearing at magnification of 1×. (B) Binary image of the superficial fascia vascularization. (C) A second binary image showing the skeleton of the superficial fascia vessels was derived from the vascular profiles in B using binary thinning procedures. Black dots: crossing point of superficial fascia vessels. Arrows: examples of segments of superficial fascial vessels
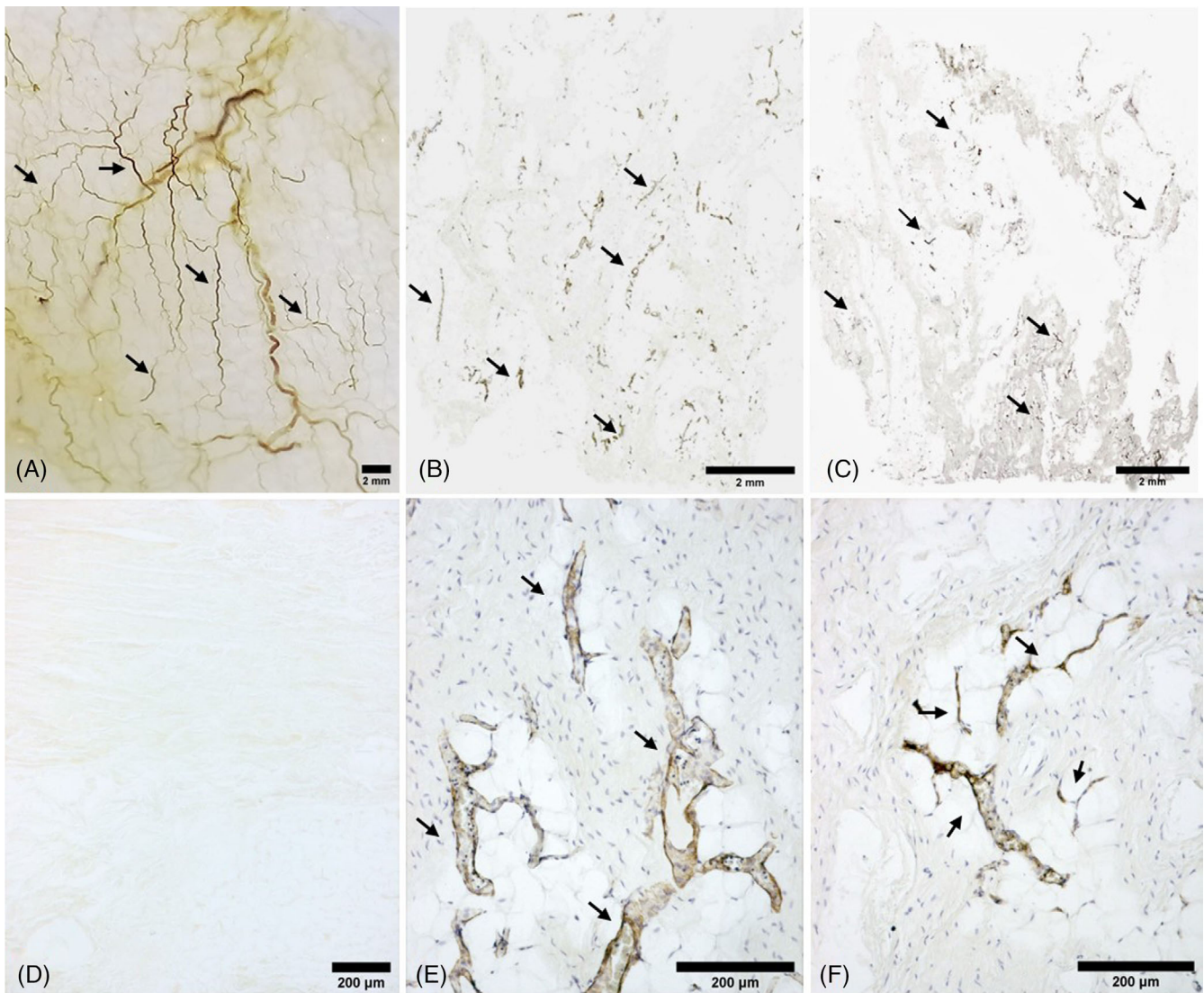

FIGURE 4 Evidence of a fine and intrigued superficial fascia vascular meshwork. (A) Superficial fascia after clearing; (B,E) αSMA staining, paraffin-embedded 5 μm section (B, scanner acquired); (C,F) von Willebrand factor staining, paraffin-embedded 5 μm section (C, scanner acquired); (D) omitted antibodies; arrows: examples of blood vessels

then derived and the branching points were identified using a binary thinning procedure. The transformation from digital to binary and skeletonized images is shown in Figure 3.

The fractal dimension (D) and lacunarity were measured to globally describe and assess the complexity of the form in quantitative terms. The D quantifies the rate at which increased magnification, scale, or resolution becomes apparent (Guidolin et al., 2004). It thus represents an index of morphological complexity: the more irregular an object, the higher its D value (Guidolin et al., 2004). It can be measured using a variety of methods but the box-counting method (Smith et al., 1996) is the most widely used in biological applications. The information provided by the D is often complemented by the measurement of lacunarity. Generally speaking, the parameter can be considered a measure of the non-uniformity (heterogeneity) of a structure, and it is potentially useful to characterize how an available space is filled (Bassingthwaighte et al., 1994). For the most part, its values tend to be higher when the structure analyzed has larger gaps.

The images from the αSMA-stained sections were examined to calculate the percentage of arterial vessels, and the images from the von Willebrand factor staining were examined to calculate the total percentage of the vessels. The following procedure was then used to estimate the percent area (Area%) occupied by the stained structures. Briefly, color deconvolution was used to identify the blood vessels. The method, which separates stains using the algorithm by Ruifrok et al. (2003), was performed by implementing an ImageJ plugin specifically developed by Gabriel Landini (see http://www.mecourse.com/landinig/software/software.html). This procedure leads to the generation of two images of vascular vessel profiles that can be easily

discriminated using conventional thresholding methods (Shen et al., 2006). A region of interest corresponding to the superficial fascia was traced, and the quantity of vessels in the superficial fascia was then evaluated by estimating the percent area (Area%) occupied by the stained structures.

Depending on the morphology of the wall, the diameters of the different types of vessels were classified as arteries, capillaries, veins or lymphatic segments and they were assessed in the von Willebrand factor- and αSMA-stained sections and in the semithin sections using an interactive procedure involving manual tracing of their thickness. Fifty measurements per section were collected to estimate this parameter.

The mean values and standard deviations of the percentage measurements were calculated. The results are reported as mean (±SD) values.

3 | RESULTS

A dense vascular meshwork was consistently identified in all the full-thickness specimens of the superficial fascia examined (Figure 4).

Histologically the superficial fascia is composed of layers of fibrous-elastic connective tissue interpenetrated by adipose clusters that is, irregular islands of thin sublayers of fat cells deposited between the layers of collagen fibers. The vasculature was characterized by a fine, dense meshwork, constituted by the different types of vessels that "run" inside the superficial fascia, both longitudinally and transversely, and also crossing it at full thickness (Figure 5). All of these vessels connect with one another, creating a rete mirabile. These vessels extend
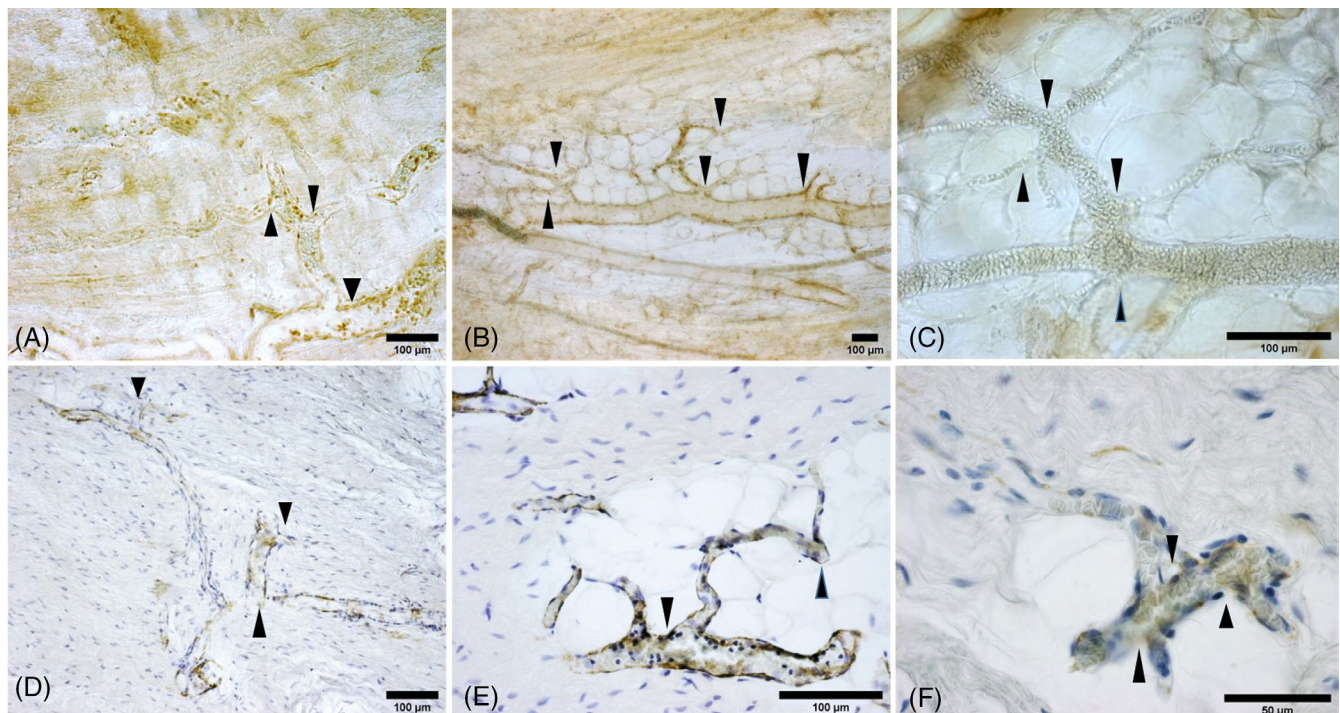

FIGURE 5 Evidence of well branched superficial fascia vasculature with segments and crossing points. (A–C) Free-floating sections, DAB (diaminobenzidine) staining; (D–F) αSMA staining, paraffin-embedded 5 μm section. Arrowheads: branching point
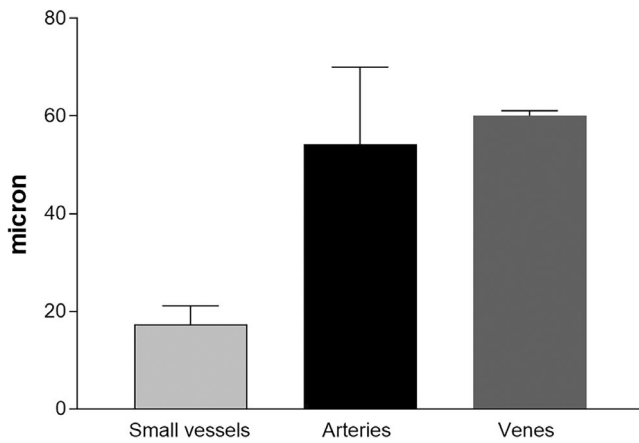
FIGURE 6 Diameters of vessels within superficial fascia: small vessels, arteries and veins

along straight as well as curved paths in close contact with the cellular and extracellular matrix component of the fascia.

The diameters of these vessels fell within a range of 13–65 μm (Figure 6). After the morphological recognition of their vascular wall in the von Willebrand factor and αSMA stainings and the semithin sections, a mean diameter of 54.24 ± 15.80 μm for the arteries (Figure 7), 60.10 ± 1.04 μm for the veins (Figure 7), 17.28 ± 3.84 μm for small vessels (vessels with a diameter less than or equal to 20 μm: capillaries and lymphatics. Figure 8) was ascertained.

Immunohistochemical analysis showed a positive reaction to S100 and Tyrosine Hydroxylase, which enveloped the arteries, indicating the existence of an autonomic innervation of the vasculature within the superficial fascia (Figure 9).

In some samples, arterio-venous anastomoses (AVAs) were identified (Figure 10). These structures showed a direct connection
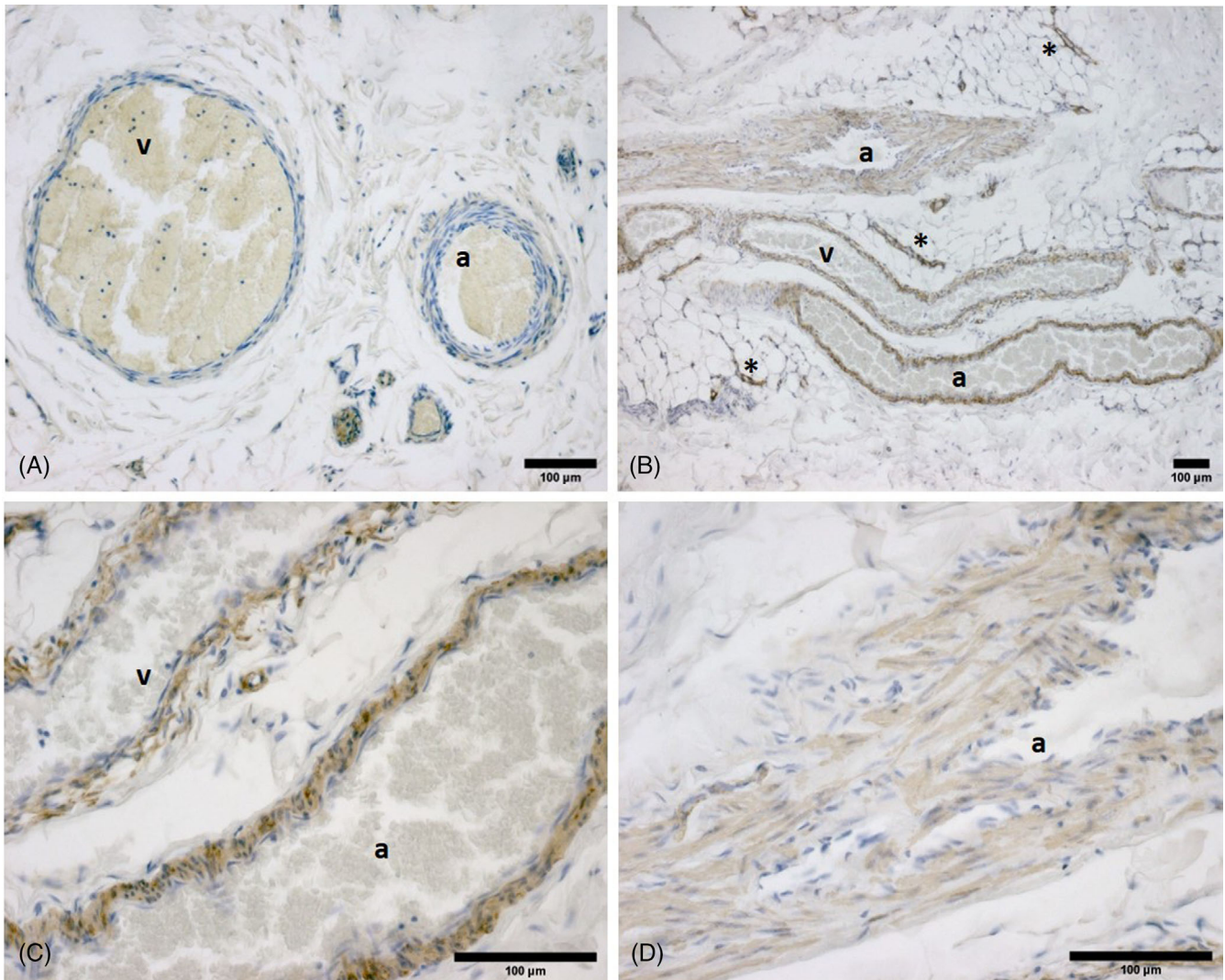

FIGURE 7 Arteries and veins. (A) Hematoxylin staining; (B–D) α-SMA staining (a = artery, v = vein); Brown staining: smooth muscle cells; *: capillaries
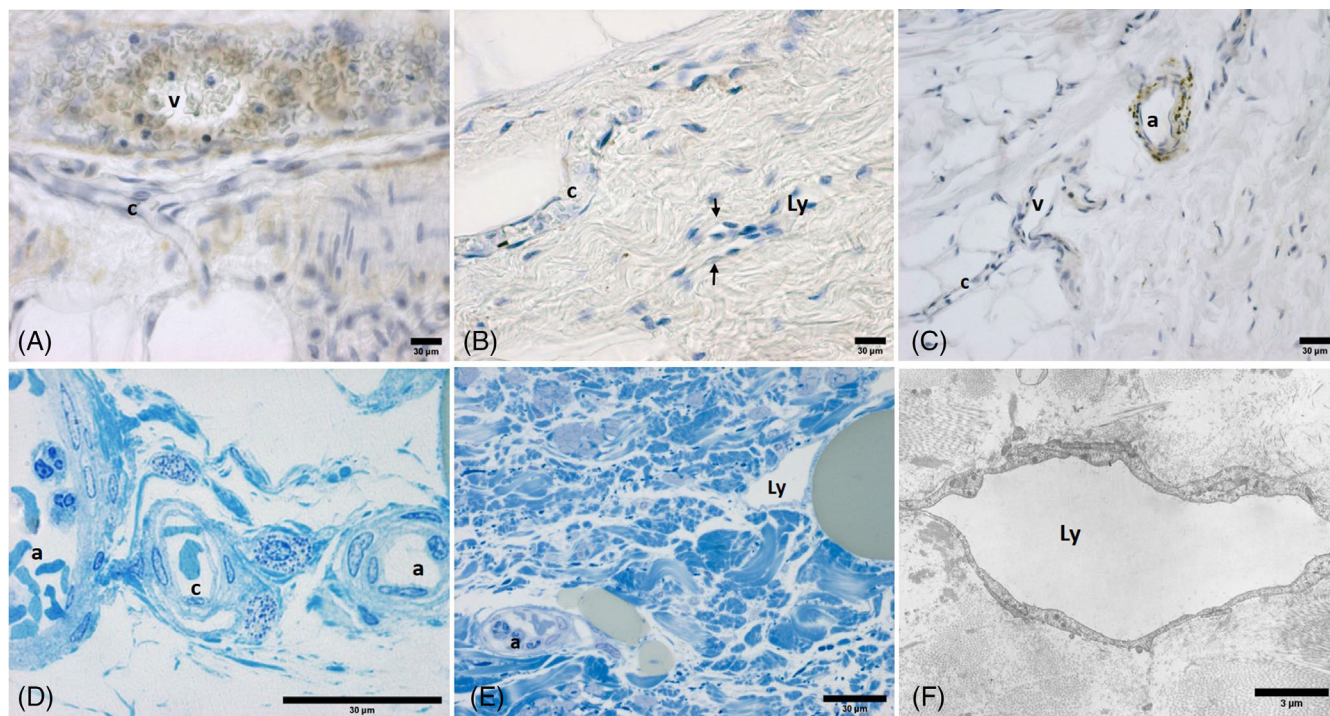
FIGURE 8 Small vessels. (A,B) Hematoxylin staining; (C) tyrosine hydroxylase staining; (D,E) semithin section (toluidine blue staining); (F) TEM analysis: lymphatic vessel. a, artery; c, capillaries; Ly and arrows: lymphatic vessel; v, vein
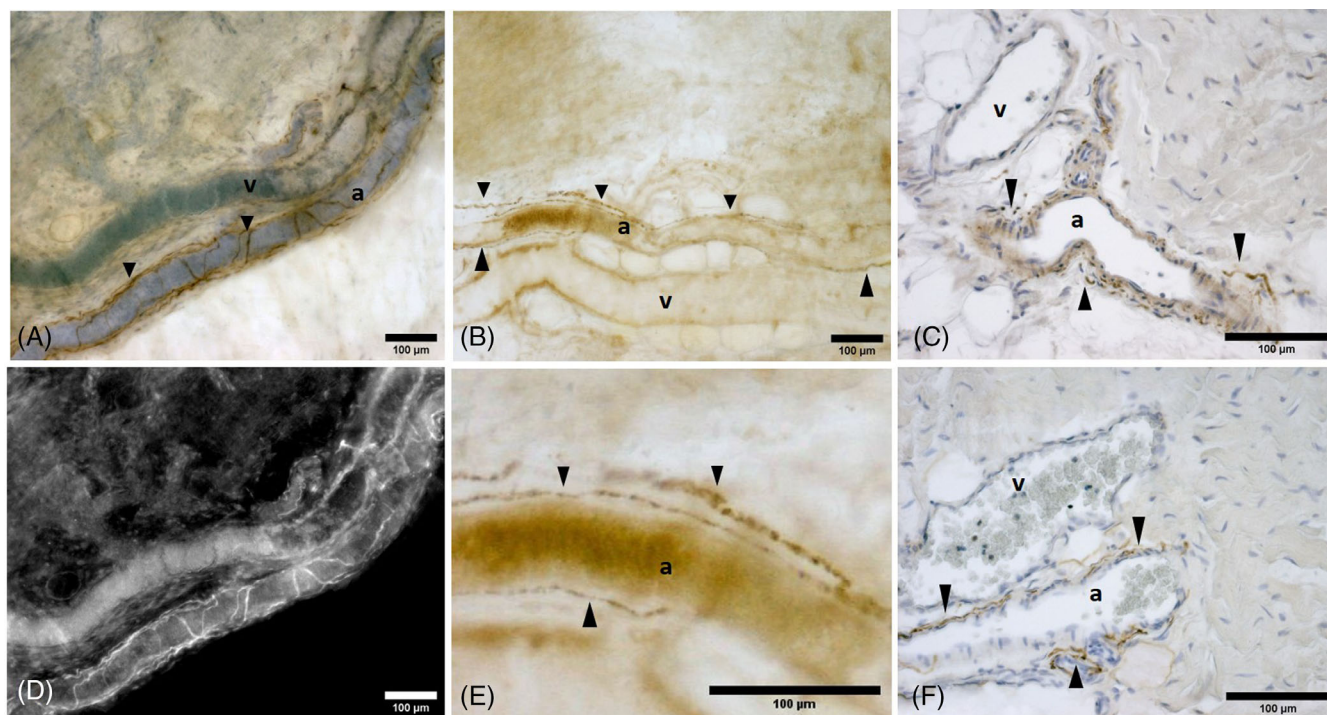

FIGURE 9 Autonomic innervation that envelopes the vessels. (A,B,D,E) Free-floating sections. (A,D) S100 staining (D, image invert color); (B,E) tyrosine hydroxylase staining; (C,F) paraffin-embedded 5 μm section, (C) tyrosine hydroxylase staining, (F) S100 Staining; arrows: innervation

between the small arteries and veins, with no capillary section between them.

In all the samples, the image processing and analysis procedure made it possible to identify vascular profiles to calculate the first topological parameter, the percentage of the superficial fascia covered by the vessels per field of view (Figure 2B). These parameters are summarized in Table 1. Globally, if we consider the area percentage of von Willebrand factor stained vessels, it represents 6.20%
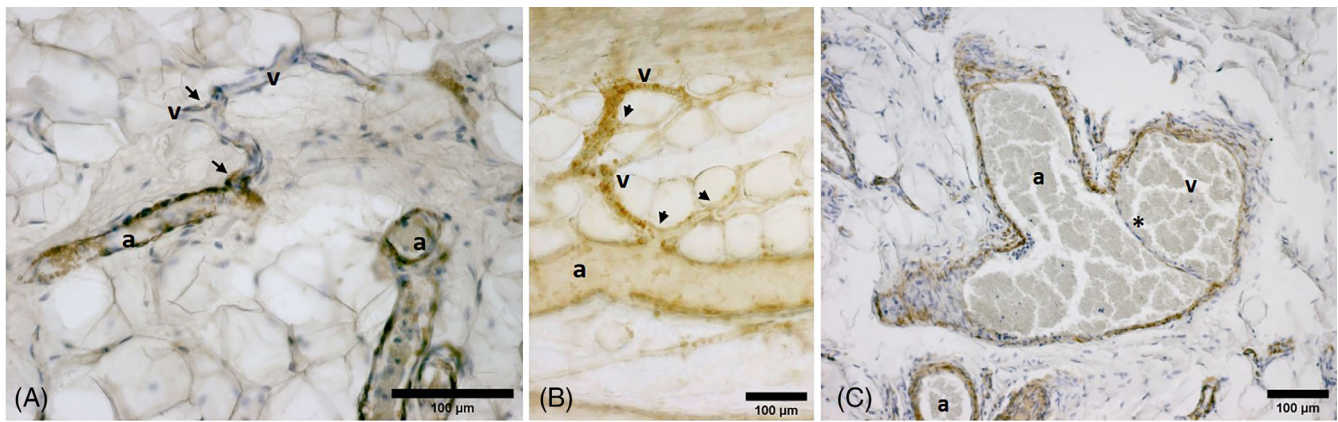
FIGURE 10 Arterio-venous anastomoses, a direct connection between small arteries and veins. (A–C) Paraffin sections, αSMA staining, (B) free-floating section, DAB (diaminobenzidine) staining; a, artery; v, venules; arrow, branching point; *, valve

± 2.10% of the total area of the superficial fascia, but if we consider only the area percentage of the αSMA-stained vessels, it is 2.93% ± 1.80%.

Topological analysis based on skeletonized superficial fascia vasculature is more sensitive than measurements of the area covered by vessels to highlight its qualitative features.

The binary image showing the skeletonized superficial fascia vessels was derived from the vascular profiles (Figure 3B) using the binary thinning procedures (Figure 3C). The skeletonized images were used to measure two other topological parameters, namely the crossing points of the superficial fascia vessels (black dots in Figure 3C) that is, all the points where vessels crossed regardless of the level of the vascular bed and a related metric, and the number of resulting vessel segments (some indicated by arrows in Figure 3C) that is, all the segments that were identified by two adjacent crossing points. The mean values of the segments were 6615 ± 3070 and 8.40 ± 3.40 per mm^2: for the crossing points they were 3092 ± 1490 and 3.40 ± 1.90 per mm^2 (Table 2). The average segment length was 4.69 ± 1.32 mm (Table 2).

As these topological parameters do not fully characterize the vascular structure, a fractal analysis of the images was also undertaken. The D and lacunarity fractal parameters, which are inversely related, are measures of the degree of structural variance. These parameters are summarized in Table 3.

4 | DISCUSSION

The aim of this study, which was based primarily on a quantitative topological and fractal analysis, was to assess data demonstrating that Scarpa'a fascia is vascularized. To our knowledge, this is the first study examining the vasculature of this structure. Until now, only general data regarding vascularization found in the skin has been reported (Standring, 2016). The results of the current study uncovered a rich, dense vascular meshwork in Scarpa's fascia with a % von Willebrand Factor immune-reactive area = 6.20 ± 2.10 and a % αSMA immune-

TABLE 1 Mean values (±standard deviation) of the % area covered by vessels within the superficial fascia

% Area (von Willebrand factor immune-reactive)	% Area (αSMA immune-reactive)
6.20 ± 2.10	2.93 ± 1.80

reactive area = 2.93 ± 1.80. The difference in percentages highlights the presence of different types of vessels.

As ultrasound imaging is able to assess the size and thickness of the superficial fascia, several studies have been able to confirm that the superficial fascia is located directly under the skin and the superficial adipose layer (Abu-Hijleh et al., 2006; Lancerotto et al., 2011; Pirri et al., 2020; Pirri, Fede, et al., 2022; Pirri, Stecco, et al., 2022). Morphologically, the superficial fascia, which shows stratification both grossly and microscopically, is the fascia layer that organizes the subcutaneous adipose tissue (Stecco et al., 2019). It is conventionally described as being made up of membranous layers with loosely packed interwoven collagen and elastic fibers (Pirri, Fede, et al., 2022; Pirri, Stecco, et al., 2022; Pirri et al., 2021).

It is known that the subcutaneous vascular system is strictly connected to the connective tissue framework of the hypodermis (Stecco, 2015). The arteries cross the hypodermis in two ways: perpendicularly and longitudinally. Perpendicularly, they cross the fascia layers and the subcutis to reach the skin (perforating arteries). Longitudinally they (the long arteries) cross the plane of the subcutis following an oblique course in the superficial fascia for long distances (Li & Ahn, 2011). The subcutaneous veins are embedded within the superficial fascia. In fact, (Caggiati, 1999) hypothesized that the lack of fascia support around the veins could be the cause of varicose veins. Hoggan (1884) affirmed that hypodermal lymphatic vessels form a web in the superficial fascia of humans.

The results of the current study are consistent with those of the works mentioned above showing that, as demonstrated by its morphological and morphometric features, the vascularization of Scarpa's fascia entails various types of vessels (arteries, veins, capillaries and

TABLE 2 Mean values (±standard deviation) of the segments, the segments for mm^2, the segment lengths (mm), the crossing points and the crossing points for mm^2 of the vessels within the superficial fascia

Patients	Segments	Segments for mm^2	Segment lengths (mm)	Crossing points	Crossing points for mm^2
1	6548 ± 3123	8.82 ± 3.60	5.73 ± 1.3	3382 ± 1682	3.36 ± 1.56
2	9130.41 ± 4212	13.02 ± 6.32	4.72 ± 1.3	4672 ± 1484	7.24 ± 2.22
3	8350 ± 3452	9.63 ± 4.34	3.48 ± 1.23	4002 ± 1312	5.04 ± 2.03
4	6936 ± 3342	8.86 ± 3.82	7.60 ± 1.34	3825 ± 1338	4.74 ± 1.94
5	3322.2 ± 1587	4.95 ± 1.93	5.36 ± 1.31	1797 ± 935	1.68 ± 0.9
6	4496 ± 2832	5.51 ± 2.21	3.72 ± 1.4	2252 ± 1567	1.76 ± 0.7
7	4533.21 ± 2121	5.33 ± 2.11	4.21 ± 1.34	2308 ± 1847	2.63 ± 1.51
	6615 ± 3070	8.40 ± 3.40	4.69 ± 1.32	3092 ± 1490	3.4 ± 1.9

lymphatic sections). The diameters of these vessels fell into a range between 13 and 65 μm (Figure 6). The large numbers of capillaries and the marked variability in the diameter of the arteries confirmed that a rete mirabile exists within the superficial fascia.

Image analysis methods made it possible to carry out a quantitative characterization of the different morphological aspects of Scarpa's fascia. As has been reported by other studies examining different types of vascularization in other organs and topographical regions, spatial statistics-based image analysis methods are available to uncover the features of these vessels and how they cooperate in any particular tissue (Guidolin et al., 2021; Kopylova et al., 2017).

An analysis of study results showed that the vascular network within Scarpa's fascia is well- branched, as confirmed by the number of the segments (6615 ± 3070 and 8.40 ± 3.40 per mm^2), crossing points (3092 ± 1490 and 3.40 ± 1.90 per mm^2), as well as by the lengths of the segments (4.69 ± 1.32 mm) uncovered by our analyses.

An analysis of the fractal dimension and the lacunarity also support the topological parameters. Those parameters are measurements of structural variance and inversely related, meaning that high values of D and low/medium values of lacunarity indicate homogeneity and a high level of structure, as was demonstrated for the retinal microvasculature by Guidolin et al. (2004). Our results (showing that D was 1.063 ± 0.10 and lacunarity was 0.60 ± 0.10) indicate that this particular vascular network is not particularly complex, exhibits a good distribution, and homogenously occupies the entire space of the superficial fascia.

Moreover, as can be seen in Figure 5, the presence of arteriovenous connections within the deep subcutaneous plexus of the superficial fascia and the marked autonomic innervation of these vessels suggest that they could play a role in thermoregulation and thus in human temperature control (Walløe, 2015) and in vascularization strategies for skin tissue engineering.

Last but not least, to date, many studies have presented examples of branching morphogenesis requiring the coordinated interplay of multiple types of epithelial cells and extracellular matrix highlighting the relationship between vascular and neuronal networks (Ribatti & Guidolin, 2020; Ribatti & Guidolin, 2022; Watts & Strogatz, 1998). This mechanism also seems to exist in the superficial fascia in view of the evidence of autonomic innervation of the blood vessels (Figure 9).

TABLE 3 Mean values (±standard deviation) of the parameters quantifying textural properties of the superficial fascia vascularization

D	Cv D	Lacunarity
1.063 ± 0.10	0.001 ± 0.0003	0.60 ± 0.10

In the light of these findings, the richness and organization of the vascularization of the superficial fascia can explain why the preservation of Scarpa's fascia during abdominoplasty is characterized by beneficial advantages over the classical abdominoplasty technique. The implications of the vascularization of the superficial fascia could include temperature regulation, which in turn could be connected to arterio-venous anastomoses, and to pain management via subcutaneous drug injection.

4.1 | Limitations of the study

The small number of patients/samples included in this single-center study cohort and the qualitative nature of its assessments do not permit us to statistically analyze the prevalence of morphological/ morphometric data. Neither can we explain cause/effect relationships, nor prognostic significance, and only indirectly therapeutic implications. The vascular composition of superficial fascia in obese patients could hypothetically be different from that of healthy individuals (Frayn & Karpe, 2014; Koenen et al., 2021; Villaret et al., 2010). Longitudinal studies including larger numbers of patients/samples are warranted if we hope to gain a clearer idea of the pathophysiology of different vasculature patterns.

5 | CONCLUSIONS

In conclusion, the study's results confirm that Scarpa's fascia is a highly vascularized tissue and they have clarified the types of vessels, topological and fractal parameters characterizing the network. Moreover, they contribute to a better understanding of the difference between the vascularization of the superficial fascia and the rest of

the subcutaneous tissue and, accordingly, explain the benefits of the preservation of Scarpa's fascia during abdominoplasty. Future studies should continue to examine the vascularization of the superficial fascia given its implications for reconstructive surgery and pain management.

ORCID

Carmelo Pirri https://orcid.org/0000-0002-0119-6549
Raffaele De Caro https://orcid.org/0000-0002-8991-7610
Carla Stecco https://orcid.org/0000-0002-8767-4555

REFERENCES

Abu-Hijleh, M. F., Roshier, A. L., Al-Shboul, Q., Dharap, A. S., & Harris, P. F. (2006). The membranous layer of superficial fascia: Evidence for its widespread distribution in the body. *Surgical and Radiologic Anatomy*, *28*(6), 606–619.

Bassinghtwaighte, J. B., Leibovitch, L. S., & West, B. J. (1994). *Fractal physiology. American Physiological Society methods in Physiology Series*. Oxford University Press.

Caggiati, A. (1999). The saphenous venous compartments. *Surgical and Radiologic Anatomy*, *21*(1), 29–34.

Das, M. K., Pandey, A., Mandal, S., Nayak, P., & Kumaraswamy, S. (2022). Modified video endoscopic inguinal lymphadenectomy: A deep-first approach. *Urology*, *168*, 234–239. https://doi.org/10.1016/j.urology.2022.06.005

de la Parra-Marquez, M., Fernandez-Riera, R., Romay-Chambers, E., & Escamilla, L. T. (2021). Superficial thinning of the DIEP flap: A safe option to achieve an aesthetic reconstructed breast in the obese patient. *Plastic and Reconstructive Surgery 1*, *148*(5), 715–719.

Fede, C., Porzionato, A., Petrelli, L., Fan, C., Pirri, C., Biz, C., De Caro, R., & Stecco, C. (2020). Fascia and soft tissues innervation in the human hip and their possible role in post-surgical pain. *Journal of Orthopaedic Research*, *38*(7), 1646–1654.

Frayn, K. N., & Karpe, F. (2014). Regulation of human subcutaneous adipose tissue blood flow. *International Journal of Obesity*, *38*(8), 1019–1026.

Guidolin, D., Tortorella, C., & Ribatti, D. (2021). Spatial statistics-based image analysis methods for the study of vascular morphogenesis. *Methods in Molecular Biology*, *2206*, 67–88.

Guidolin, D., Vacca, A., Nussdorfer, G. G., & Ribatti, D. (2004). A new image analysis method based on topological and fractal parameters to evaluate the angiostatic activity of docexatel by using the Matrigel assay in vitro. *Microvascular Research*, *67*, 117–124. https://doi.org/10.1016/j.mvr.2003.11.002

Hoggan, G. (1884). On multiple lymphatic nævi of the skin, and their relation to some kindred diseases of the lymphatics. *Journal of Anatomy and Physiology*, *18*(3), 304–326.

Iwanaga, J., Singh, V., Ohtsuka, A., Hwang, Y., Kim, H. J., Moryś, J., Ravi, K. S., Ribatti, D., Trainor, P. A., Sañudo, J. R., Apaydin, N., Şengül, G., Albertine, K. H., Walocha, J. A., Loukas, M., Duparc, F., Paulsen, F., Del Sol, M., Adds, P., … Tubbs, R. S. (2021). Acknowledging the use of human cadaveric tissues in research papers: Recommendations from anatomical journal editors. *Clinical Anatomy*, *34*(1), 2–4.

Koenen, M., Hill, M. A., Cohen, P., & Sowers, J. R. (2021). Obesity, adipose tissue and vascular dysfunction. *Circulation Research*, *128*(7), 951–968.

Kopylova, V. S., Boronovskiy, S. E., & Nartsissov, Y. R. (2017). Fundamental principles of vascular network topology. *Biochemical Society Transactions*, *45*(3), 839–844.

Koshima, I., Inagawa, K., Jitsuiki, Y., Tsuda, K., Moriguchi, T., & Watanabe, A. (1996). Scarpa's adipofascial flap for repair of wide scalp defects. *Annals of Plastic Surgery*, *36*, 88–92.

Koshima, I., & Saeda, S. (1989). Inferior epigastric artery skin flaps without rectus abdominis muscle. *British Journal of Plastic Surgery*, *42*(6), 645–648.

Lancerotto, L., Stecco, C., Macchi, V., Porzionato, A., Stecco, A., & De Caro, R. (2011). Layers of the abdominal wall: Anatomical investigation of subcutaneous tissue and superficial fascia. *Surgical and Radiologic Anatomy*, *33*(10), 835–842.

Li, W., & Ahn, A. C. (2011). Subcutaneous fascial bands: A qualitative and morphometric analysis. *PLoS One*, *6*(9), e23987.

Macchi, V., Porzionato, A., Stecco, C., Tiengo, C., Parenti, A., Cestrone, A., & De Caro, R. (2011). Body parts removed during surgery: A useful training source. *Anatomical Sciences Education*, *4*(3), 151–156. https://doi.org/10.1002/ase.218

Macchi, V., Tiengo, C., Porzionato, A., Stecco, C., Galli, S., Vigato, E., Azzena, B., Parenti, A., & De Caro, R. (2007). Anatomo-radiological study of the superficial musculo-aponeurotic system of the face. *Italian Journal of Anatomy and Embryology*, *112*(4), 247–253.

Moon, H. K., & Taylor, G. I. (1988). The vascular anatomy of rectus abdominis musculocutaneous flaps based on the deep superior epigastric system. *Plastic and Reconstructive Surgery*, *82*(5), 815–832.

Mori, H., Akita, K., & Hata, Y. (2007). Anatomical study of innervated transverse rectus abdominis musculocutaneous and deep inferior epigastric perforator flaps. *Surgical and Radiologic Anatomy*, *29*(2), 149–154.

Novais, C. S., Carvalho, J., Valença-Filipe, R., Rebelo, M., Peres, H., & Costa-Ferreira, A. (2020). Abdominoplasty with Scarpa fascia preservation: Randomized controlled trial with assessment of scar quality and cutaneous sensibility. *Plastic and Reconstructive Surgery*, *146*(2), 156–164.

Odobescu, A., & Keith, J. N. (2021). Preshaping DIEP flaps: Simplifying and optimizing breast reconstruction aesthetics. *Plastic and Reconstructive Surgery*, *147*(5), 1059–1061.

Pirri, C., Fede, C., Petrelli, L., Guidolin, D., Fan, C., De Caro, R., & Stecco, C. (2021). An anatomical comparison of the fasciae of the thigh: A macroscopic, microscopic and ultrasound imaging study. *Journal of Anatomy*, *238*(4), 999–1009.

Pirri, C., Fede, C., Petrelli, L., Guidolin, D., Fan, C., De Caro, R., & Stecco, C. (2022). Elastic Fibres in the subcutaneous tissue: Is there a difference between superficial and muscular fascia? *A cadaver study. Skin Research and Technology*, *28*(1), 21–27.

Pirri, C., Fede, C., Pirri, N., Petrelli, L., Fan, C., De Caro, R., & Stecco, C. (2021). Diabetic foot: The role of fasciae, a narrative review. *Biology*, *10*(8), 759.

Pirri, C., Stecco, A., Fede, C., De Caro, R., Stecco, C., & Özçakar, L. (2020). Ultrasound imaging of a scar on the knee: Sonopalpation for fascia and subcutaneous tissues. *European Journal of Translational Myology*, *30*(1), 150–153.

Pirri, C., Stecco, C., Petrelli, L., De Caro, R., & Özçakar, L. (2022). Reappraisal on the superficial fascia in the subcutaneous tissue: Ultrasound and histological images speaking louder than words. *Plastic and Reconstructive Surgery*, *150*, 244–245.

Ribatti, D., & Guidolin, D. (2020). Branching morphogenesis—Historical first evidences. *The International Journal of Developmental Biology*, *64*(9), 397–407.

Ribatti, D., & Guidolin, D. (2022). Morphogenesis of vascular and neuronal networks and the relationships between their remodeling processes. *Brain Research Bulletin*, *1*(186), 62–69.

Ruifrok, A. C., Katz, R. L., & Johnston, D. A. (2003). Comparison of quantification of histochemical staining by hue-saturation-intensity (HSI) transformation and color-deconvolution. *Applied Immunohistochemistry & Molecular Morphology*, *11*, 85–91.

Scarpa, A. (1809). *Sull'ernie: memoire anatomico-chirurgiche*. Stamperia Reale.

Scarpa A. (1823). *Traité Pratique des Hernies*. Gabon, Paris.

Schneider, C. A., Rasband, W. S., & Eliceiri, K. W. (2012). NIH image to ImageJ: 25 years of image analysis. *Nature Methods*, *9*, 671–675. https://doi.org/10.1038/nmeth.2089

Shen, W. Y., Lai, C. M., Graham, C. E., Binz, N., Lai, Y. K., Eade, J., Guidolin, D., Ribatti, D., Dunlop, S. A., & Rakoczy, P. E. (2006). Long-term global retinal microvascular changes in a transgenic vascular endothelial growth factor mouse model. *Diabetologia*, *49*(7), 1690–1701.

Smith, T. G., Lange, G. D., & Marks, W. B. (1996). Fractal methods and results in cellular morphology-dimensions, lacunarity and multifractals. *Journal of Neuroscience Methods*, *69*, 123–136.

Southern, S., & Ramakrishnan, V. (1996). Re: Scarpa's adipofascial flap for repair of wide scalp defects. *Annals of Plastic Surgery*, *37*, 343–344.

Standring, S. (2016). *Gray's anatomy: The anatomical basis of clinical practice* (41st ed.). Elsevier Churchill Livingstone.

Stecco, C. (2015). *Functional atlas of the human fascial system*. Elsevier Health Sciences.

Stecco, C., & Duparc, F. (2011). Fasciae anatomy. *Surgical and Radiologic Anatomy*, *33*(10), 833–834.

Stecco, C., Pirri, C., Fede, C., Fan, C., Giordani, F., Stecco, L., Foti, C., & De Caro, R. (2019). Dermatome and fasciatome. *Clinical Anatomy*, *32*(7), 896–902.

Villaret, A., Galitzky, J., Decaunes, P., Estève, D., Marques, M. A., Sengenès, C., Chiotasso, P., Tchkonia, T., Lafontan, M., Kirkland, J. L., & Bouloumié, A. (2010). Adipose tissue endothelial cells from obese human subjects: Differences among depots in angiogenic, metabolic, and inflammatory gene expression and cellular senescence. *Diabetes*, *59*(11), 2755–2763.

Walløe, L. (2015). Arterio-venous anastomoses in the human skin and their role in temperature control. *Temperature*, *3*(1), 92–103.

Watts, D. J., & Strogatz, S. H. (1998). Collective dynamics of 'small-world' networks. *Nature*, *393*(6684), 440–442.